AIP Journal of Applied Physics

Zoned near-zero refractive index fishnet lens antenna: Steering millimeter waves

V. Pacheco-Peña, B. Orazbayev, U. Beaskoetxea, M. Beruete, and M. Navarro-Cía

Citation: Journal of Applied Physics **115**, 124902 (2014); doi: 10.1063/1.4869436
View online: http://dx.doi.org/10.1063/1.4869436
View Table of Contents: http://scitation.aip.org/content/aip/journal/jap/115/12?ver=pdfcov
Published by the AIP Publishing

Zoned near-zero refractive index fishnet lens antenna: Steering millimeter waves

V. Pacheco-Peña,[1,a)] B. Orazbayev,[1,b)] U. Beaskoetxea,[1,c)] M. Beruete,[1,d)] and M. Navarro-Cía[2,3,4,e)]
[1]*TERALAB (MmW—THz—IR & Plasmonics Laboratory), Universidad Pública de Navarra, Campus Arrosadía, 31006 Pamplona, Spain*
[2]*Optical and Semiconductor Devices Group, Department of Electrical and Electronic Engineering, Imperial College London, London SW7 2BT, United Kingdom*
[3]*Centre for Plasmonics and Metamaterials, Imperial College London, London SW7 2AZ, United Kingdom*
[4]*Centre for Terahertz Science and Engineering, Imperial College London, London SW7 2AZ, United Kingdom*

(Received 5 February 2014; accepted 13 March 2014; published online 25 March 2014)

A zoned fishnet metamaterial lens is designed, fabricated, and experimentally demonstrated at millimeter wavelengths to work as a negative near-zero refractive index lens suitable for compact lens antenna configurations. At the design frequency $f = 56.7$ GHz ($\lambda_0 = 5.29$ mm), the zoned fishnet metamaterial lens, designed to have a focal length FL $= 9\lambda_0$, exhibits a refractive index $n = -0.25$. The focusing performance of the diffractive optical element is briefly compared with that of a non-zoned fishnet metamaterial lens and an isotropic homogeneous zoned lens made of a material with the same refractive index. Experimental and numerically-computed radiation diagrams of the fabricated zoned lens are presented and compared in detail with that of a simulated non-zoned lens. Simulation and experimental results are in good agreement, demonstrating an enhancement generated by the zoned lens of 10.7 dB, corresponding to a gain of 12.26 dB. Moreover, beam steering capability of the structure by shifting the feeder on the *xz*-plane is demonstrated. © *2014 AIP Publishing LLC*. [http://dx.doi.org/10.1063/1.4869436]

I. INTRODUCTION

After more than a decade of intensive research, metamaterial concepts are now being applied in a variety of fields, though the main impulse is still in electromagnetism, where they were first proposed[1] and demonstrated.[2] They have enabled numerous applications thanks to the artificial manipulation of the material intrinsic electromagnetic properties.[3]

The field of lenses has greatly benefited from metamaterials since their initial conception. The perfect lens,[4] superlenses,[5] hyperbolic lenses,[6–8] and advanced lenses designed on the basis of transformation optics[9,10] or extreme refractive index values[11–13] show the merits of applying metamaterials concepts throughout the whole spectrum. Different metamaterial implementations have been proposed for lenses to fulfill the particular requirements of each spectral window. For microwaves, the classical arrangement of split ring resonators and wires has been widely used.[14,15] However, for higher frequencies, these structures are limited due to their increasing losses. Therefore, for higher frequencies, such as millimeter-waves, the fishnet metamaterial is the preferred choice.[11,16,17] The fishnet metamaterial consists of stacked subwavelength hole arrays working in the extraordinary transmission realm.[18–22] Hence, it is also known as extraordinary transmission metamaterial.[23]

One of the drawbacks of the lenses studied in Refs. 11, 12, 16, and 17 is that they are bulky, due to the need of several layers to realize the desired profile/performance. This was overcome in Ref. 24 by simply zoning the lens, which implies the removal of layers each time a critical thickness is reached, resulting in a reduced volume/weight and, additionally, lower insertion losses.

Here, the study of the zoned fishnet metamaterial lens presented in Ref. 24 is extended and it is focused on the radiation characteristics when the diffractive optical metamaterial element is fed by an ideal omnidirectional feeder or a real open-ended waveguide. Moreover, the steering capability of the lens is demonstrated experimentally and compared with numerical simulations. The structure is designed to work at the frequency $f = 56.7$ GHz ($\lambda_0 = 5.29$ mm) with a focal length FL $= 47.62$ mm $= 9\lambda_0$. From the dispersion diagram of an infinite fishnet metamaterial, at the design frequency, the structure behaves as a near-zero refractive index medium (also called zero index materials, ZIM) with $n = -0.25$.

II. METAMATERIAL ZONED LENS DESIGN

The numerical study of the zoned lens is made using the commercial software CST Microwave Studio™. First, the eigenmode solver of the software is used to compute the effective refractive index of an infinite fishnet metamaterial whose unit cell is shown in the inset of Fig. 1(a). The dimensions of the unit cell are $d_x = 3$ mm, $d_y = 5$ mm, $d_z = 1.5$ mm (air gap of 1 mm and metal thickness $w = 0.5$ mm), and hole diameter $a = 2.5$ mm. Perfect electric conductor is used for this simulation since it is a good approximation for metals at millimeter-waves and simplifies the analysis. With these

[a)]Electronic mail: victor.pacheco@unavarra.es
[b)]Electronic mail: b.orazbayev@unavarra.es
[c)]Electronic mail: unai.beaskoetxea@unavarra.es
[d)]Electronic mail: miguel.beruete@unavarra.es
[e)]Electronic mail: m.navarro@imperial.ac.uk

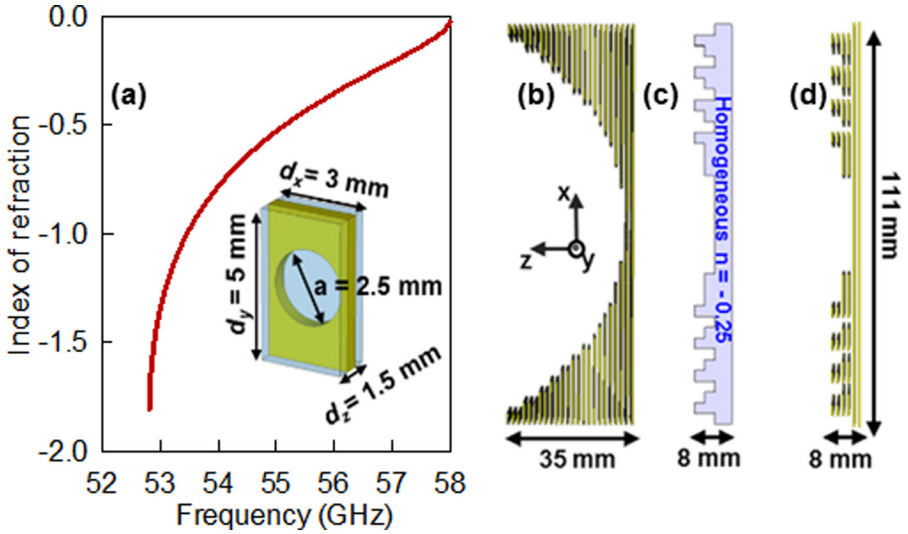

FIG. 1. (a) Effective refractive index, n_z, of an infinite fishnet metamaterial; (inset) schematic representation of the unit cell with dimensions: $d_x = 3$ mm, $d_y = 5$ mm, $d_z = 1.5$ mm, metal thickness $w = 0.5$ mm and hole diameter $a = 2.5$ mm. Schematic representation of the different profiled lenses studied in this work: (b) concave profile using the fishnet metamaterial, (c) zoned lens using an isotropic homogeneous medium with $n = -0.25$, and (d) zoned lens using the fishnet metamaterial.

conditions, a single hole has its cut-off frequency at 72 GHz. However for an array of such holes, extraordinary transmission appears in the range between 53 and 58 GHz. It has been demonstrated in the past that extraordinary transmission resonance is caused by the accumulation of energy in the vicinity of the first order diffraction mode cutoff, thus it is directly related to the periodicity of the hole matrix.[20,22] The simulation result of the effective n_z for the fundamental band is shown in Fig. 1(a). It can be observed that the fishnet metamaterial is dispersive with negative refractive index at the fundamental band. We choose $f = 56.7$ GHz ($\lambda_0 = 5.29$ mm) as the design frequency, where $n = -0.25$ [see Fig. 1(a)], because the dispersion is lower in such ZIM regime.

According to the general equation of conical curves, for $n = -0.25$ and one face flat, the lens profile of the remaining face needs to be an ellipse.[11] Although this planoconcave profile [Fig. 1(b)] is thinner than the convex profiles of dielectric lenses, it is still slightly bulky and precludes the use of the fishnet metamaterial lens for applications with space limitation, such as automotive radar systems. This disadvantage can be overcome by zoning the lens, whereby parts of the lens are removed when their phase variation with respect to free-space propagation is an integer multiple of 2π.[24,25] This determines a thickness limit (t) that can be mathematically calculated as a relation between the free-space wavelength (λ_0) and the effective refractive index of the structure, as follows:

$$t = \frac{\lambda_0}{1-n}. \tag{1}$$

Note that, due to the selected refractive index of the fishnet metamaterial ($n = -0.25$), $t = 0.8\lambda_0 \approx 4.23$ mm, i.e., it is smaller than the free-space wavelength, allowing us to design a compact lens.

By combining the general equation of an ellipse[11] and the thickness limit from Eq. (1), the equation for the zoned profile of the lens is obtained as follows:[24]

$$(1-n^2)(z+mt)^2 - 2(FL+mt)(1-n)(z+mt) + x^2 = 0, \tag{2}$$

where m is an integer representing the successive steps for the zoned lens profile ($m = 0, 1, 2, 3$).

By choosing a focal length, FL = 47.62 mm = $9\lambda_0$, the final lens profile obtained following Eq. (2) is shown on Figs. 1(c) and 1(d). The whole structure comprises a total number of 37×27 holes along x and y directions, respectively, and between 2 and 6 stacked plates along z-axis. Thus, the metal structure of the lens can be enclosed by a box with dimensions $21\lambda_0 \times 25.5\lambda_0 \times 1.5\lambda_0$.[24] Notice that the total thickness of $1.5\lambda_0$ is not in contradiction with Eq. (1), since Eq. (1) accounts for the thickness limit corresponding to the zoned face. The total thickness, however, is composed of such thickness and the additional holey plate at the back of the lens.

III. SIMULATION RESULTS

In this section, the zoned fishnet metamaterial lens is compared numerically with two more idealized lenses to evaluate its performance: a non-zoned fishnet metamaterial lens and an isotropic homogenous zoned lens with effective index $n = -0.25$, see Figs. 1(b) and 1(c). First, the focusing properties of the three lenses are studied when they are illuminated from their flat interface by an ideal plane-wave. Afterwards, the radiation pattern of the zoned lens is compared with its non-zoned counterpart when a point feeder (short electric dipole) at the focal point is used to excite the lens.

To begin with, the output profile of the non-zoned fishnet metamaterial lens is obtained by using Eq. (2) with $m = 0$, resulting a lens with a concave-profiled output face. The homogenous lens is simulated using the frequency-domain solver of CST Microwave Studio™. We are interested in evaluating the performance of the homogeneous structure for a single frequency ($f = 56.7$ GHz); therefore, by using this solver, the structure is simulated without the need of a dielectric dispersion model, such as Drude material to mimic the ZIM behavior. This way, simulation time is reduced. Moreover, periodic boundary conditions are imposed along y so that the lens is effectively infinite in that direction, whereas open boundary conditions (i.e., perfectly

matched layers) are used along x and z. The other designs (non-zoned and zoned fishnet metamaterial lenses) are simulated using the transient solver in order to evaluate the spectral response of the lenses within the millimeter-wave V-band (see Sec. IV). The excitation is done with a vertically polarized (E_y) plane-wave impinging on the flat face of the structures.

Simulation results of the spatial power distribution in xz-plane for the three structures at the working frequency $f = 56.7$ GHz ($\lambda_0 = 5.29$ mm) are shown in Fig. 2. It is evident that they all work as focusing lenses and that they have similar focal lengths: the non-zoned lens has FL = 47.4 mm ($=8.96\lambda_0$) which is very close to the homogenized zoned lens FL = 47.63 mm ($=9.01\lambda_0$), whereas the zoned lens presents a slightly different value, FL = 49.5 mm ($=9.35\lambda_0$). The small difference ($0.34\lambda_0 = 3.7\%$) between the ideal FL obtained with the isotropic homogeneous structure and the zoned fishnet metamaterial lens validates the design here presented.

The power distribution at the focal plane for each lens is presented on top of each two-dimensional color map. The full width at half maximum (FWHM) along x at the focal plane is very similar in all considered cases, namely, $0.47\lambda_0$, $0.57\lambda_0$, and $0.56\lambda_0$ for the non-zoned, zoned, and homogenized lenses, respectively. Moreover, it can be observed that the lateral lobes are more prominent for both zoned lenses. This is as expected due to the smaller output numerical aperture of the zoned lenses compared with the non-zoned case. However, these simulation results demonstrate that the zoned fishnet metamaterial lens does not exhibit major deterioration on the overall performance.

Regarding the radiation pattern, the lens is compared numerically with its non-zoned counterpart, using three-dimensional lenses. A short electric dipole is used as feeder and is placed at the focal length obtained from Fig. 2. Far-field monitors are used to record the radiation pattern of the two lenses within the frequency range 50–60 GHz with a step of 0.5 GHz. Note that this is an approximated study because of the chosen feeder. This is done in order to evaluate the performance of the fishnet metamaterial lenses when an idealized excitation (omnidirectional) is used. In Sec. IV, a realistic study will be presented using an open-ended waveguide (WR-15) as feeder.

The simulation results for the power distribution of the co- and cross-polar components on the H-plane are presented in Figs. 3(a) and 3(b) and Figs. 3(c) and 3(d) for the non-zoned and zoned structures, respectively. It is shown that the co-polar enhancement (defined as the ratio between the power available when the lens is used and the power received without the lens) of the non-zoned lens (12.9 dB) is slightly better than that of the zoned lens (11.2 dB). Hence, the directivity (defined as the ratio between the radiated power density in the direction of maximum emission, 0° in our case, and the power density radiated by an ideal isotropic source emitting the same total power) obtained with the non-zoned and zoned lens is 15.17 dBi and 14.53 dBi, respectively. The cross-polarization at 0° of the non-zoned and zoned structures is −180 dB and −178 dB at the design frequency. In addition, cross-polar lobes appear at ±43° and ±37.2° for the non-zoned and zoned lenses, respectively, at the design frequency ($f = 56.7$ GHz). They are more prominent for the zoned lens with a level of 144.9 dB and 142.2 dB

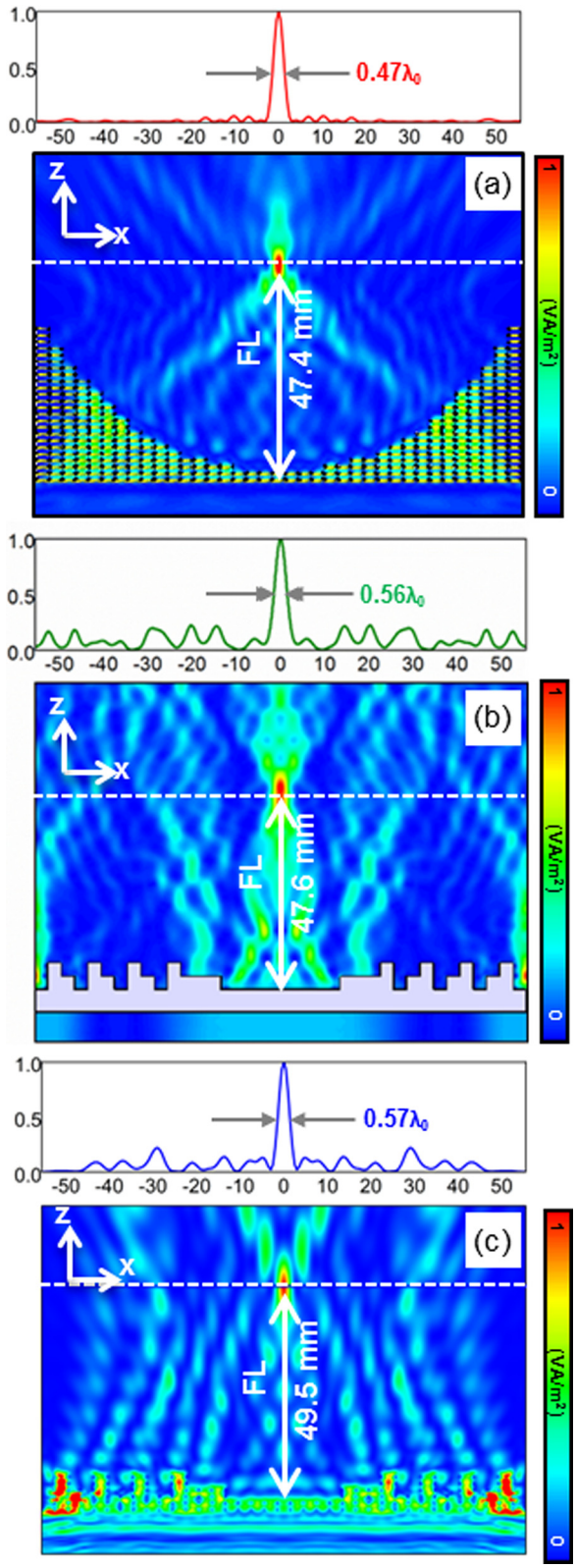

FIG. 2. Normalized spatial power distribution in xz-plane: (a) non-zoned fishnet metamaterial lens, (b) zoned lens using an isotropic homogeneous medium with $n = -0.25$, and (c) zoned fishnet metamaterial lens. The top panel of each figure is the power at the focal length along the white dashed line (x-axis in mm) depicted in each two-dimensional color map.

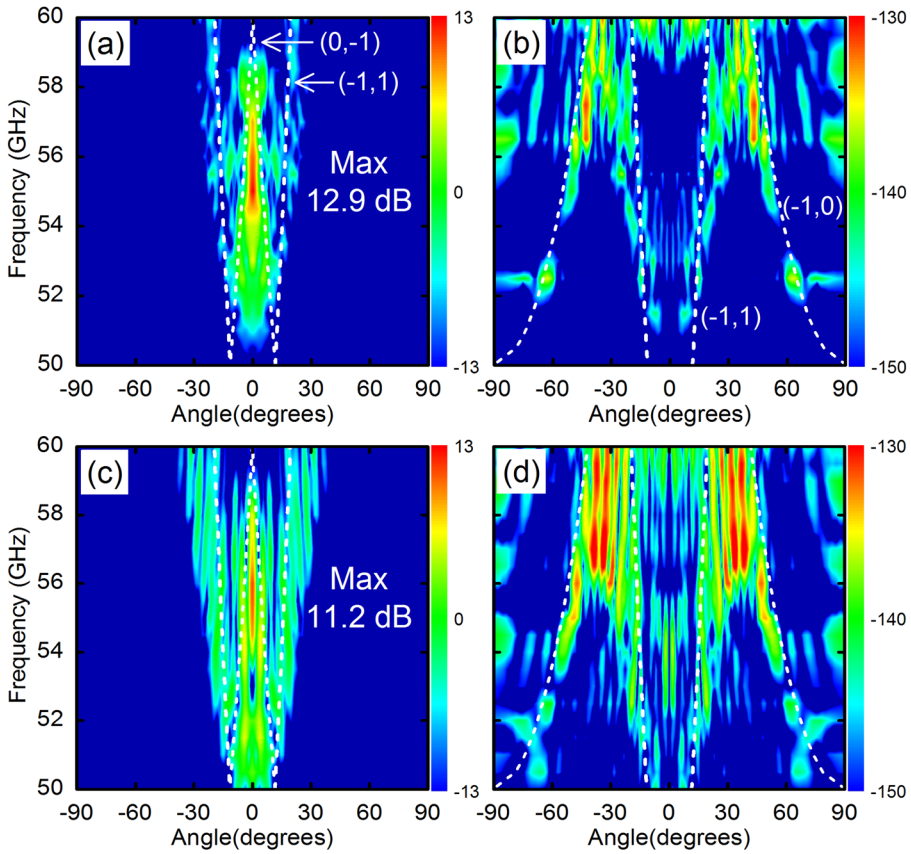

FIG. 3. Simulation results of radiation pattern (dB) for the frequency range 50–60 GHz using a point source at the focal position: co-polarization (a) and (c) and cross-polarization (b) and (d) of the non-zoned (a) and (b) and zoned (c) and (d) fishnet metamaterial lens antenna. The white dashed lines represent the analytical positions of the grating lobes of order (0,−1), (−1,0), and (−1,1).

below the co-polar for the non-zoned and zoned cases, respectively [see Figs. 3(b) and 3(d)]. The origin of these side lobes and those also observed for the co-polar around ±15–20° can be arguably assigned to grating lobes, as the white dashed lines in Fig. 3 demonstrate.

This better performance of the non-zoned lens can be explained on the basis of the spillover efficiency (i.e., the ratio between the power reemitted from the lens and the total power radiated by the feed; this parameter gives an idea of the total power radiated from the source that is intercepted by the lens). According to the simulations, the spillover efficiency (η_{so}) is 0.25 and 0.19 for the non-zoned and zoned lenses, respectively. However, these results again corroborate that the zoned fishnet metamaterial lens has a small deterioration on its properties compared to the non-zoned counterpart.

IV. EXPERIMENTAL RESULTS: RADIATION PATTERN

The zoned fishnet metamaterial lens was fabricated using aluminum layers perforated and cut by laser. Frames of the same metal with thickness of 1 mm were used to create the air gap between each holey plate. A picture of the fabricated zoned fishnet metamaterial lens is presented in Fig. 4(a). Measurements of the zoned lens were performed using an ABmm™ millimeter-wave quasi-optical vector network analyzer (VNA) in the V-band. To evaluate the radiation characteristics of the lens, the radiation pattern was measured following the next procedure: an open-ended rectangular waveguide (WR-15) was placed at the experimental focal length (FL = 46.5 mm = 8.79λ_0), see Sec. III and Ref. 22, to excite the lens. Both elements, open-ended waveguide and lens, were standing on a rotating platform in order to make angular measurements from −90° to +90°, with a step of 1°. A high gain standard horn antenna was placed at 4000 mm from the flat face of the lens to detect the radiated power. The schematic representation of the experimental setup is presented in Fig. 4(b) along with the pictures of the open-ended waveguide [Fig. 4(c)] and the horn antenna [Fig. 4(d)] used as feeder and detector, respectively. First, a calibration of the system was made by recording the transmitted power in absence of the lens. Next, the lens was placed between detector and feeder.

In order to better assess the performance of the fabricated lens, simulations were also launched for the three-dimensional non-zoned and zoned fishnet structures by using a realistic open-ended WR-15 as feeder at the numerically-estimated focal point. As it was done in Sec. III, far-field monitors were used to record the radiation pattern of the two lenses within the frequency range 50–60 GHz with a step of 0.5 GHz. The simulation results for the power distribution of the co- and cross-polar components on the H-plane are presented in Figs. 5(a) and 5(b) and Figs. 5(c) and 5(d) for the non-zoned and zoned structures, respectively. Experimental measurements for the co- and cross-polarizations are presented in Figs. 5(e) and 5(f), respectively.

By inspection of the measurement and the simulation results from Fig. 5 along with the simulations from Fig. 3, it is evident that the use of a realistic waveguide feeder models significantly better the experiment. The spillover efficiency is now 0.9 and 0.86 for the non-zoned and zoned lens, respectively, and arguably can explain the closer performance between the non-zoned and zoned lens.

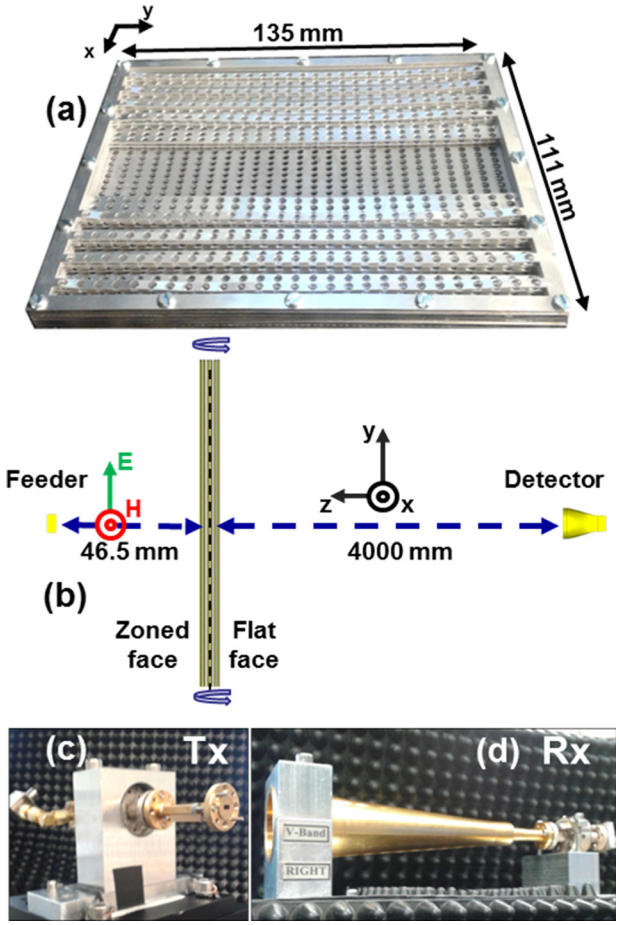

FIG. 4. (a) Picture of the fabricated zoned fishnet metamaterial lens. (b) Schematic representation of the experimental set-up for the characterization of the radiation pattern. (c) Open-ended rectangular waveguide used as feeder and (d) horn antenna used as detector.

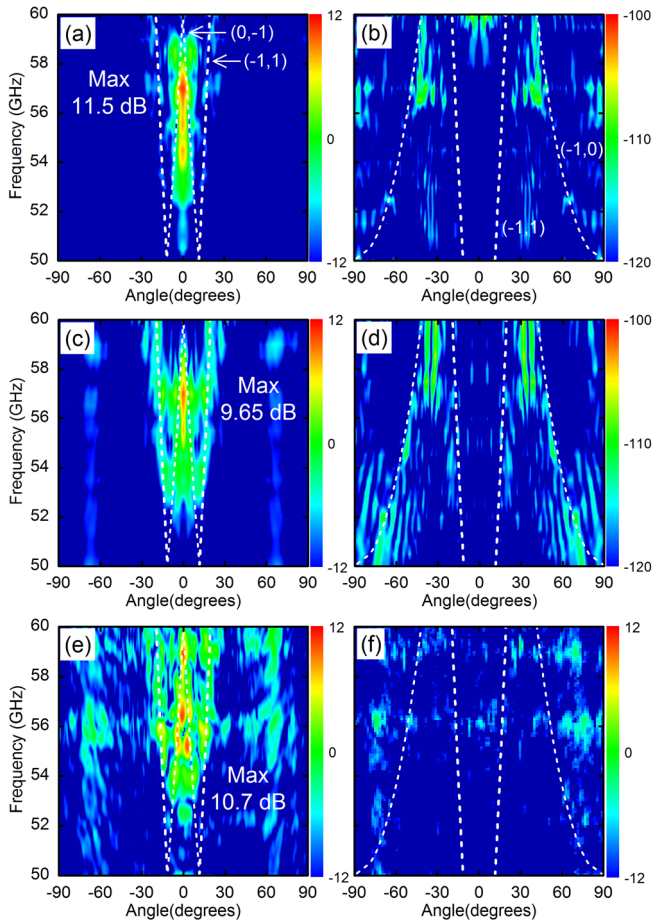

FIG. 5. Radiation pattern (dB) for the frequency range 50–60 GHz: simulation results for co-polarization (left column) and cross-polarization (right column) of the non-zoned (a) and (b) and zoned (c) and (d) fishnet metamaterial lens; experimental co-polarization (e) and cross-polarization measurements (f) of the zoned fishnet metamaterial lens; the white dashed lines represent the analytical positions of the grating lobes of order (0,−1), (−1,0), and (−1,1).

A high enhancement of the zoned lens is obtained in the experiment (10.7 dB), which is slightly better than the simulation value (9.65 dB), see Figs. 5(c) and 5(e). A very narrow *H*-plane beamwidth is found ($\theta_{-3\,\mathrm{dB}} = 3.5°$), demonstrating its good performance. Notice that the minor discrepancy between simulation and experiment falls within the experimental error. The enhancement of the non-zoned lens (11.5 dB)—obtained uniquely from simulation—is slightly better than that of the zoned lens, in good agreement with the numerical results of Sec. III. In the zoned lens, the co-polar component presents side lobes near ±70°, which are observed in both simulation and experimental results within the whole frequency range, with a magnitude between −12 and −10 dB (i.e., −22.7–−20.7 dB relative to the main lobe) in the experiment, see Fig. 5(e). In the simulation, they have slightly smaller values, see Fig. 5(c). These side lobes are due to the spillover. Hence, they are frequency independent. Given the larger numerical aperture of the non-zoned lens, these side lobes are not present [see Fig. 5(a)]. All this is more evident by looking at the radiation pattern of both non-zoned and zoned lenses for $f = 56.7$ GHz [see Figs. 6(a) and 6(b), respectively]. The zoned lens has clearly such prominent side lobes at ±70°, whereas the non-zoned lens has such side lobes due to spillover at ±90° with a magnitude near −16 dB (−27 dB relative to the main lobe). A simple approach to reduce spillover side lobes in the zoned lens would be to decrease the focal length-to-diameter ratio.

It is known that side lobes can also be generated due to periodicity, so called grating lobes. They are unavoidable in our lenses because of the fishnet periodic nature. The analytical positions of the first order grating lobes (0,−1), (−1,0), and (−1,1) are plotted as white dashed lines in Fig. 5, revealing clearly the origin of all the side lobes observed in the diagram. Note that when a short electric dipole was used as feeder in last section, grating lobes were also observed (see Fig. 3).

To facilitate comparison, the normalized radiation diagram of the zoned lens at the design frequency ($f = 56.7$ GHz) is shown in Fig. 6(c), for simulation results of the co-polarization (dotted line) and experimental measurements (solid lines). The cross-polar level at 0° is −43 dB, whereas the simulation predicts the unmeasurable −209 dB (notice that we have estimated the dynamic range of the system to be ∼50 dB). Meanwhile, the simulations predict cross-polar lobes at ±39.2° and ±34° at the design frequency for the non-zoned and zoned lenses, respectively. However, since their magnitudes are below the noise floor of the system, they are not recorded in the experiment.

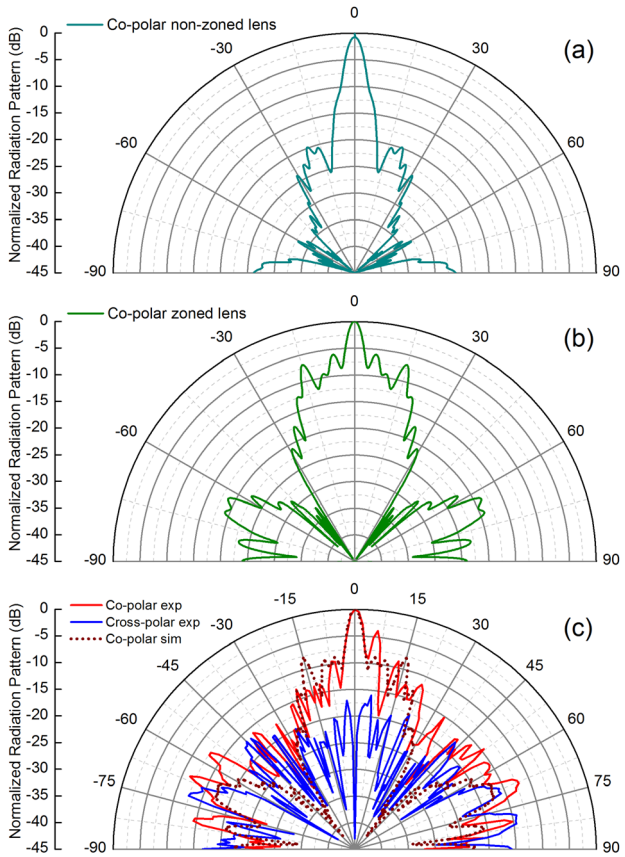

FIG. 6. Simulation results of the radiation pattern (dB) at the design frequency ($f = 56.7$ GHz) for the co-polarization of the non-zoned (a) and zoned lens (b). (c) Simulation (dotted curve) and experimental results (solid curves) for the normalized power at the design frequency ($f = 56.7$ GHz): co-polarization (red curve) and cross-polarization (blue curve).

In order to fully characterize the radiation performance, the numerically-computed and experimental gain (defined as the ratio of the radiated power density in the direction of maximum emission, 0° in our case, and the power density radiated by an ideal lossless isotropic radiator that emits all the power fed by the source) for the zoned fishnet metamaterial lens are presented in Fig. 7 in the frequency range of 50–60 GHz. For the experiment, the gain is obtained comparing our lens antenna with a horn antenna following the gain comparison method.[26] A high gain of 12.26 dB is found, close to the value obtained in simulation (14.9 dB), which is directly calculated by using the software-implemented far-field monitors. As happened with the enhancement, the gain is slightly better for the non-zoned lens (16.5 dB; not shown in the plot). The small difference between simulation and

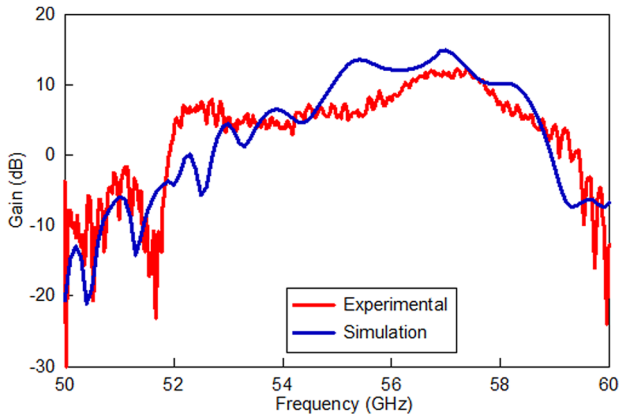

FIG. 7. Gain of the zoned fishnet metamaterial lens (dB) for the frequency range 50–60 GHz: simulation (blue curve) and experimental measurement (red curve).

experimental results obtained can be due to the imperfections on the fabrication and assembly of the lens. In general, simulation and experimental results are in good agreement.

The results obtained in this section for the zoned lens are summarized in Table I: −3dB beamwidth in the *H*-plane, cross-polar level at 0°, gain, cross-polar main lobe location, comparing simulation and experiment.

V. BEAM STEERING USING THE ZONED FISHNET METAMATERIAL LENS

Following the analysis of the radiation pattern of the zoned lens, its beam steering capability by mechanical shift of the feeder is studied in this section.

According to Fourier optics, the output beam can be steered in a lens antenna by shifting the feeder.[27] Therefore, we aim to find experimentally in the first instance the coordinates on the *xz*-plane where the feeder should be placed in order to steer the output angle from 0° to 20° in 5° steps. Next, we characterize the radiation properties of the steerable beam.

The process to find experimentally the position on the *xz*-plane of the open-ended waveguide feeder is as follows: first, the whole system is fixed at each measured output angle (0°, 5°, 10°, 15° and 20°). Then, the feeder is moved on the *xz*-plane in order to find the position at which the maximum power is detected. The feeder is moved from 0 to 15 mm and from 20 to 70 mm along *x*-axis and *z*-axis, respectively, with a step of 0.5 mm. In this way, the focal point coordinates on the *xz*–plane are obtained accurately.

TABLE I. Simulations and experimental results of the radiation performance.

Structure	BW[a]	Cross-polar at 0° (dB)	Location ML[b] cross-polar (deg)	ENH[c] (dB)	G[d] (dB)
Non-zoned lens (simulation)	3.6	−203	±39.2	11.5	16.5
Zoned lens (simulation)	3.8	−209	±34	9.65	14.9
Zoned lens (experimental)	3.5	−43	Not detected due to the limit of dynamic range	10.7	12.26

[a]BW is the *H*-plane beamwidth.
[b]ML is the main lobe.
[c]ENH is the enhancement.
[d]G is the gain.

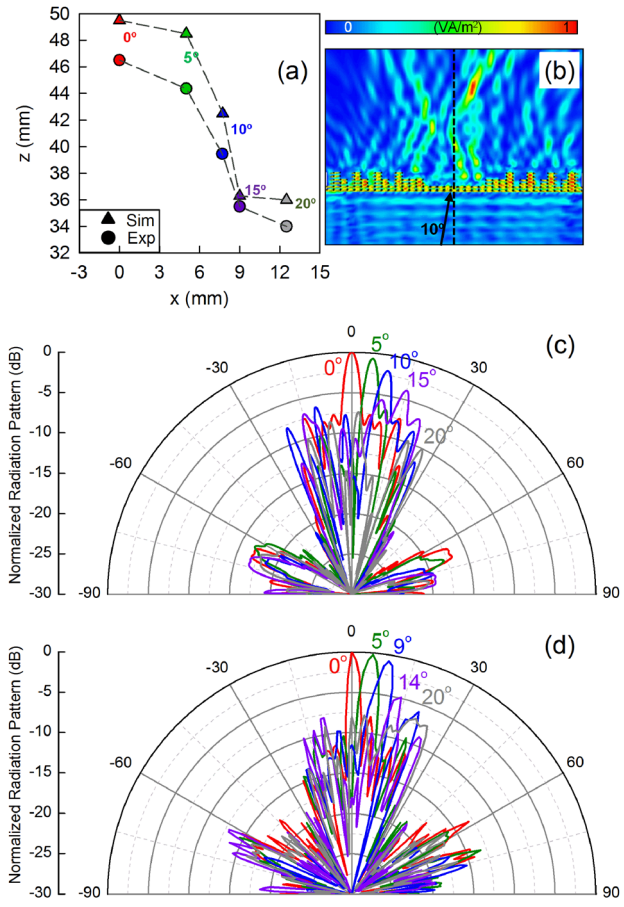

FIG. 8. (a) (x,z) coordinates of the focal length on the xz-plane for the output angles 0°, 5, 10°, 15°, and 20°: simulation results (filled-triangles) and experimental positions (filled-circles). (b) Simulation result of the spatial power distribution on the xz-plane when a plane wave impinges obliquely at 10° upon the flat-input face of the zoned fishnet metamaterial lens. Results of the radiation pattern for the angles obtained at the output of the lens: (c) simulation and (d) experimental results.

The experimental positions of the open-ended waveguide found, for each output angle, by the above described procedure are shown in Fig. 8(a) as filled circles. By invoking reciprocity, the shifting of the focal position can be also numerically computed by exciting the zoned lens with a plane-wave at the desirable oblique incidence. This is illustrated in Fig. 8(b), where simulation of the spatial power distribution on the xz-plane is presented when a plane-wave impinges obliquely at 10° upon the flat-input face of the lens. Following this approach, the simulation results (filled triangles) of the (x,z) coordinates of the focal position when a plane-wave impinges obliquely with different angles (0°, 5°, 10°, 15°, and 20°) are also presented in Fig. 8(a). Note that the experimental positions are slightly different from the simulation coordinates, yet the trend is maintained. This small discrepancy can be assigned to experimental tolerances, such as the accuracy of the feeder position.

Simulation and experimental results of the radiation pattern at the design frequency for the output angles 0°, 5°, 10°, 15°, and 20° are presented in Figs. 8(c) and 8(d), respectively. Simulations are now done by placing the open-ended WR-15 at the numerically-estimated positions [filled triangles in Fig. 8(a)]. It is shown that the experimental output angles are indeed very close to the values obtained by simulations.

To summarize the beam characteristics regarding the mechanical beam steering using the fabricated zoned fishnet metamaterial lens, the results of the output angles, beamwidth at −3 dB for the H-plane, and the side lobe level are presented in Table II for simulation and experimental results. From the comparison of these results, one can observe that experimental and simulation results are in good agreement for all output angles, except for 20° where a clear deterioration in terms of beamwidth and side lobe level is obtained. The beamwidth in the H-plane for simulation and experiment shows a range between 3° and 4° for all output angles, except for 20° where beamwidth is 8°. Moreover, it can be seen that the lower side lobe level is obtained for the output angle 0° and 5° for simulation and experiment, respectively. Note that the difference between the experimental beamwidth for 0° and 5° is however only 12.5% and falls within the experimental error. Furthermore, the experimental side lobe level for the output angle 20° is only 1.56 dB below the main lobe. Compared with simulations, the side lobe level at the angle 20° is 5.4 dB. This discrepancy can be due to errors in the location of the feeder for experimental measurements. Based on these results, and considering a scan loss of 3 dB (which is commonly used for evaluating the steering capability of an antenna; scan loss is defined as the maximum value of power reduction allowed for a given angle compared with the value at 0°), the structure here designed has a beam steering capability up to ±10°.

VI. CONCLUSIONS

In this paper, a zoned fishnet metamaterial lens was designed, simulated, and measured at millimeter-waves. The performance of the zoned lens was compared with a non-

TABLE II. Simulations and experimental results of the beam steering capability.

Output angles (deg)		H-plane beamwidth (deg)		Side lobe level (dB)	
Simulational	Experimental	Simulational	Experimental	Simulational	Experimental
0	0	3.8	3.5	7.5	7.93
5	5	3.6	4	6.1	8
10	9	4	4	5.7	5.76
15	14	4.3	4	5.6	4.71
20	20	3.3	8	5.4	1.56

zoned planoconcave lens synthesized by the fishnet metamaterial and with an idealized zoned lens made of an isotropic homogeneous medium with $n = -0.25$. The radiation pattern of the zoned fishnet metamaterial lens demonstrated an experimental enhancement, compared with an open-ended WR-15 waveguide, up to 10.7 dB for the co-polarization with a gain of 12.26 dB. Meanwhile, the cross-polarization was 43 dB lower than the co-polar component at the design frequency. Finally, the beam steering capability of the zoned lens was analyzed. By changing the position of the open-ended waveguide feeder from the focal point on the *xz*-plane, experimental measurements showed that the main lobe of the radiation pattern shifted at the angles 0°, 5°, 9°, 14°, and 20°, which were very close to the required angles. Moreover, a suitable beam steering up to 10° was demonstrated by considering a standard 3 dB scan loss.

ACKNOWLEDGMENTS

In memoriam Professor Mario Sorolla.

This work was supported in part by the Spanish Government under contract Consolider Engineering Metamaterials CSD2008-00066 and Contract No. TEC2011-28664-C02-01. V.P.-P. is sponsored by Spanish Ministerio de Educación, Cultura y Deporte under Grant No. FPU AP-2012-3796. B.O. is sponsored by Spanish Ministerio de Economía y Competitividad under Grant No. FPI BES-2012-054909. M.B. is sponsored by the Spanish Government via RYC-2011-08221. M. N.-C. is supported by the Imperial College Junior Research Fellowship.

[1]V. G. Veselago, Sov. Phys. Usp. **10**, 509 (1968).
[2]D. R. Smith, W. J. Padilla, D. C. Vier, S. C. Nemat-Nasser, and S. Schultz, Phys. Rev. Lett. **84**, 4184 (2000).
[3]R. Marqués, F. Martín, and M. Sorolla, *Metamaterials with Negative Parameters: Theory, Design and Microwave Applications* (Wiley, Hoboken, NJ, 2008).
[4]J. B. Pendry, Phys. Rev. Lett. **85**, 3966 (2000).
[5]N. Fang, H. Lee, C. Sun, and X. Zhang, Science **308**, 534 (2005).
[6]Z. Liu, H. Lee, Y. Xiong, C. Sun, and X. Zhang, Science **315**, 1686 (2007).
[7]A. Monti, F. Bilotti, A. Toscano, and L. Vegni, Opt. Commun. **285**, 3412 (2012).
[8]N. Engheta and R. Ziolkowski, *Metamaterials:Physics and Engineering Explorations*, 1st ed. (John Wiley & Sons & IEEE Press, Piscataway, NJ, USA, 2006), p. 440.
[9]A. Demetriadou and Y. Hao, IEEE Antennas Wireless Propag. Lett. **10**, 1590 (2011).
[10]D.-H. Kwon and D. H. Werner, IEEE Antennas Wireless Propag. Lett. **8**, 1115 (2009).
[11]M. Navarro-Cía, M. Beruete, I. Campillo, and M. Sorolla, IEEE Trans. Antennas Propag. **59**, 2141 (2011).
[12]M. Navarro-Cía, M. Beruete, M. Sorolla, and N. Engheta, Phys. Rev. B **86**, 165130 (2012).
[13]V. Torres, V. Pacheco-Peña, P. Rodríguez-Ulibarri, M. Navarro-Cía, M. Beruete, M. Sorolla, and N. Engheta, Opt. Express **21**, 9156 (2013).
[14]C. G. Parazzoli, R. B. Greegor, J. A. Nielsen, M. A. Thompson, K. Li, A. M. Vetter, M. H. Tanielian, and D. C. Vier, Appl. Phys. Lett. **84**, 3232 (2004).
[15]R. B. Greegor, C. G. Parazzoli, J. A. Nielsen, M. A. Thompson, M. H. Tanielian, and D. R. Smith, Appl. Phys. Lett. **87**, 091114 (2005).
[16]M. Navarro-Cía, M. Beruete, I. Campillo, and M. Sorolla, Phys. Rev. B **83**, 115112 (2011).
[17]M. Beruete, M. Navarro-Cía, M. Sorolla, and I. Campillo, Opt. Express **16**, 9677 (2008).
[18]S. Zhang, W. Fan, N. C. Panoiu, K. J. Malloy, R. M. Osgood, and S. R. J. Brueck, Phys. Rev. Lett. **95**, 137404 (2005).
[19]G. Dolling, C. Enkrich, M. Wegener, C. M. Soukoulis, and S. Linden, Science **312**, 892 (2006).
[20]M. Beruete, M. Sorolla, I. Campillo, J. S. Dolado, L. Martín-Moreno, J. Bravo-Abad, and F. J. García-Vidal, Opt. Lett. **29**, 2500 (2004).
[21]M. Beruete, M. Sorolla, and I. Campillo, Opt. Express **14**, 5445 (2006).
[22]M. Navarro-Cía, M. Beruete, M. Sorolla, and I. Campillo, Opt. Express **16**, 560 (2008).
[23]M. Beruete, M. Navarro-Cía, M. Sorolla, and I. Campillo, Phys. Rev. B **79**, 195107 (2009).
[24]V. Pacheco-Peña, B. Orazbayev, V. Torres, M. Beruete, and M. Navarro-Cía, Appl. Phys. Lett. **103**, 183507 (2013).
[25]W. E. Kock, Proc. IRE **34**, 828 (1946).
[26]ANSI/IEEE Standard 149-1979, *IEEE Standard Test Procedures for Antennas* (IEEE Antennas and Propagation Society, 1979).
[27]A. Demetriadou and Y. Hao, Opt. Express **19**, 19925 (2011).